JOURNAL OF MATERIALS SCIENCE **40** (2005) 4893–4898

Interconnect thermal expansion matching to solid oxide fuel cells

B. C. CHURCH, T. H. SANDERS, JR., R. F. SPEYER, J. K. COCHRAN
School of Materials Science and Engineering, Georgia Institute of Technology, 771 Ferst Drive, Atlanta, GA 30332-0245

A method for the rapid fabrication of homogeneous potential interconnect alloys from metal oxide precursors and evaluation of their thermal expansion mismatch to solid oxide fuel cells is described. Pastes of metal oxide powders were extruded into honeycomb geometries and sintered in hydrogen. Thermal expansion mismatch was evaluated based on heating with a zero-mismatch at room temperature, and on cooling with zero-mismatch temperatures at 600 or 1100°C. The non-linear expansion behavior of Fe-Ni invar alloys resulted in different compositions being optimum, based on the assumed zero-mismatch temperature.

1. Introduction

A solid oxide fuel cell (SOFC) is a device that generates electric power through the oxidation of a fuel such as hydrogen or methane. There has been significant recent activity in developing new SOFC designs and incorporating new materials with the general goals of increasing efficiency, lowering production cost, and increasing reliability. The recent ability to operate a SOFC at relatively low temperatures (<700°C) has made it possible to economically employ metal alloys as interconnects. This is widely seen as a method to reduce cost and improve manufacturability, since metal alloys are less expensive and more formable than traditional $LaCrO_3$ interconnects. The properties that a metal interconnect should exhibit for a planar SOFC design have been recently discussed by Linderoth *et al.* [1] and Zhu and Deevi [2]; the two most critical properties are a close thermal expansion match with the electrolyte, and oxidation resistance at the operating temperature of the SOFC. Reviews of potential alloys suitable for this application have recently been made by Quadakkers *et al.* [3] and Yang *et al.* [4]. Research on SOFC interconnect alloys has tended to concentrate on oxidation behavior; several commercial and experimental ferritic Fe-Cr alloys have been identified as oxidation resistant in these reviews.

The traditional SOFC fabrication method consists of assembling alternating layers of anode, interconnect, electrolyte and cathode at room temperature [5]. The layers are stacked to create the desired cell height and seals, such as compression, glass, or cement, are applied to the edges of the plate to make the stack hermetic. Certain types of seals require a high-temperature heat-treatment during which the layers become rigidly joined while other seals become rigid upon application at room temperature. Recently, Rauch *et al.* [6] have described a method for producing hybrid SOFC stacks by means of a paste extrusion technique. The SOFC structure is comprised of alternating layers of electrolyte and metal interconnect, made from the co-extrusion of two pastes. The interconnect paste is comprised of metal oxides blended in proportion to yield the desired metal alloy composition. After co-extrusion, the SOFC stack is heat-treated in a hydrogen atmosphere in which the metal oxides that constitute the interconnect layers reduce, densify and homogenize. The yttria-stabilized zirconia (YSZ) electrolyte is chemically stable in the reducing atmosphere and only undergoes densification. The anode, cathode, gas manifolds, and contacts are added in post-heat-treatment stages. In service, SOFCs of various designs will not typically be exposed to temperatures in excess of roughly 700°C, which is the operating temperature of the fuel cell.

Eisele [7] and Cochran *et al.* [8] have examined processing defects that can occur during the heat-treatment of the hybrid SOFC stack. While certain defects can be minimized or eliminated by changing particle sizes and distributions of the raw materials, defects associated with differential contraction of the interconnect and electrolyte layers upon cooling from the sintering temperature (∼1200°C) can only be modified by changing the metal composition. Therefore, the thermal expansion behavior of the metal interconnect must be tailored to match that of the electrolyte.

Allowable mismatch in thermal expansion between SOFC materials has been mentioned [1, 9], though the proposed design limits are not generally in agreement. For traditional SOFCs, the evolution of stress due to thermal expansion mismatch would depend on the fabrication method; interfacial stress would develop on heating for stacks rigidly joined at room temperature or on cooling for stacks joined during the high-temperature heat-treatment required for certain types of seals. For hybrid SOFCs, interfacial stress initiates upon cooling at a temperature below which atomic diffusion, plastic flow, and microstructural recrystallization processes in the metal layers can relieve such stresses.

The current work details a method for rapidly fabricating interconnect alloy compositions from metal oxide precursors and characterizing their thermal expansion behavior. Extrusions of interconnect alloys can be tested independently for properties such as thermal expansion, sintering characteristics, and oxidation resistance. Potential interconnect alloys that show superior properties can then be incorporated into the more complex hybrid structure for further evaluation. The thermal expansion matching between selected Fe-Ni alloys and YSZ are compared with a commonly-recommended [4, 10] interconnect alloy, Fe 20 wt% Cr. Binary Fe-Ni alloys would likely suffer severe oxidation in the operating environment of a SOFC. This work considers only thermal expansion and is thus a first-step in the process of designing novel ternary (or greater) alloys for hybrid SOFC interconnects.

2. Experimental procedure

Metal oxides [Fe_2O_3 (Pea Ridge, 2–8 μm, 99.7%), NiO (Ceramic Color, 6 μm, 99.9%) and Cr_2O_3 (Fisher Scientific, 2–5 μm, 99.9%)] were mixed in proportion to produce the desired alloy compositions after complete reduction. The metal oxide powders were first dry-mixed with Methocel A4M (Dow Chemical), which acts as a binder when hydrated. A solution of deionized water with 2.5 wt% Pegosperse 100S (Lonza), a lubricant, was then added to the dry powder mixture in a commercially available food blender. Solids loading was kept constant at 50.5 vol% for each composition. Binder contents were tailored to meet particular paste properties using equations and techniques described by Hurysz [11]. A granulated powder mixture was produced after mixing for 30 s the blender. Next, the granulated powder was pugged in a Buss kneader to form a homogeneous paste. The paste was then formed into a honeycomb structure using a Loomis extruder with custom-made extrusion dies of various cross-sections. The extrudate was allowed to dry at room temperature for ∼24 h. Extrusions were reduced and sintered in flowing H_2 in a closed-ended tube furnace heated at a rate of 2°C/min and held at 1300°C for 10 h. Ultra high purity grade hydrogen was backfilled three times after mechanical pump evacuation and then continuously flowed through the furnace, exiting through a bubbler to prevent back diffusion of air. Honeycomb made of 8 mol% yttria-stabilized zirconia was formed using this same process, with the exception that the solids content was 40 vol% and sintering was carried out in static air in a bottom-loading $MoSi_2$ resistance element furnace.

The honeycomb samples were cut from the green extrusions prior to reduction and sintering to form a 2 × 3-type cell structure, as shown in Fig. 1. Samples were then cut to length (34.7 mm) and ground to ensure parallel ends. Dilatometry experiments were performed in a dual pushrod dilatometer using alumina pushrods/casing and a sapphire reference. A flowing argon atmosphere was used to prevent excessive oxidation of the samples. Three pump-down/backfill cycles were performed prior to each run. All experiments used a 3°C/min heating rate up to 1300°C. Data were not collected during cooling. Sample temperature was measured using a thermocouple junction floating ∼ 1 mm above the sample.

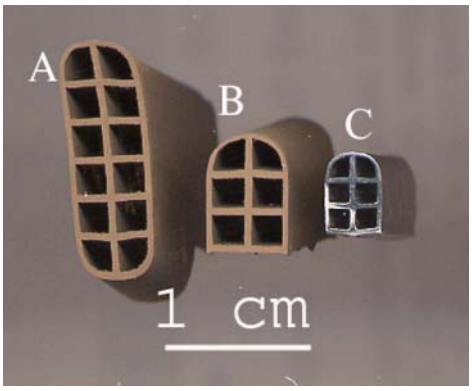

Figure 1 Cross-sections of honeycomb samples (A) as-extruded and dried, (B) cut into 2 × 3 cell geometry, and (C) as-reduced.

The coefficient of thermal expansion (CTE), α_T, was calculated from the displacement versus temperature data and is given in Equation 1

$$\alpha_T = \frac{\mathrm{d}l/l_0}{\mathrm{d}T} = \frac{1}{l_0}\frac{\mathrm{d}l}{\mathrm{d}T} \tag{1}$$

where T is temperature in °C, l_0 is the length at room temperature, and l is the length at a given temperature. It should be noted that the values of α_T may vary from other calculated values of CTE, as has been described recently by James *et al*., [12]. With the $\Delta l/l_0$ versus T data, values of α_T were calculated by linear regressions over small temperature intervals, as shown in Equation 2,

$$\alpha_T = \frac{n\sum x_i y_i - \sum x_i \sum y_i}{n\sum x_i^2 - \left(\sum x_i\right)^2} \tag{2}$$

where x_i represents a T datum point, y_i represents a $\Delta l/l_0$ datum point, and n is the range over which each regression is performed. The value of $n = 41$ was used in all calculations which roughly equates to a 20°C temperature range. The value of α_T calculated for each regression was assigned to the median temperature for each particular regression range.

An averaged CTE over a designated temperature range was calculated using Equation 3.

$$\alpha_m = \frac{1}{l_0}\frac{\Delta l}{\Delta T} \tag{3}$$

α_m is more commonly reported than α_T; in this work, values of α_m are based on a reference temperature of 20°C.

The thermal expansion mismatch between an alloy and YSZ upon heating from the zero-mismatch point of room temperature to a temperature T, $\Delta E_{T,\mathrm{heating}}$, was calculated from the raw expansion data using Equation 4.

$$\Delta E_{T,\mathrm{heating}} = \left[\frac{\Delta l}{l_0}\right]_{\mathrm{metal},T} - \left[\frac{\Delta l}{l_0}\right]_{\mathrm{YSZ},T} \tag{4}$$

The thermal expansion mismatch between an alloy and YSZ from a zero-mismatch temperature of T_S (600 or 1100°C) to a lower temperature T was calculated from Equation 5.

$$\Delta E_{T,\text{cooling}} = \left(\left[\frac{\Delta l}{l_0} \right]_{\text{metal},T} - \left[\frac{\Delta l}{l_0} \right]_{\text{metal},T_S} \right) - \left(\left[\frac{\Delta l}{l_0} \right]_{\text{YSZ},T} - \left[\frac{\Delta l}{l_0} \right]_{\text{YSZ},T_S} \right) \quad (5)$$

This equation is based on the assumption that there is a zero-stress state between the metal and YSZ at and above T_S, due to plastic flow in the metal at all higher temperatures.

Lattice parameters were calculated using the Nelson-Riley method for X-ray diffraction (XRD) data taken with a Philips PW1800 diffractometer using Cu Kα radiation. The compositions of the metal alloys were determined by first calculating the lattice parameter and then determining the composition based on literature data of lattice parameter versus composition [13]. The conversion equations used were

$$C = -2162.0 + 6115.6 \cdot a, \quad 28 < C < 38 \text{ wt\% Ni} \quad (6a)$$

$$C = 2862.1 - 7838.8 \cdot a, \quad 43 < C < 100 \text{ wt\% Ni} \quad (6b)$$

where C represents the calculated composition in wt% Ni and a represents the measured lattice parameter in nm. Diffraction and microscopy samples were in the form of extruded strip of roughly 0.5 mm thickness. Metallographic samples were prepared using standard techniques and were observed using a Leica optical microscope.

3. Results

A representative microstructure of Fe-Ni alloys made from reduced metal oxides is shown in Fig. 2. The unetched sample taken from extruded Fe 50 wt% Ni honeycomb reveals the porosity commonly observed in these materials. Pores tended to be well-rounded and had average diameters on the order of 5 μm. Porosity levels, measured by calculating the area fraction of pores from optical micrographs, ranged between 3 and 5 vol%, and showed no discernible trend with alloy composition.

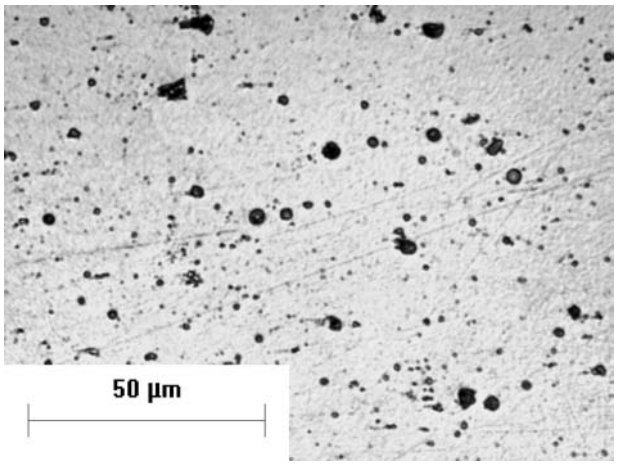

Figure 2 As-polished transverse section of Fe 50 wt% Ni metal honeycomb.

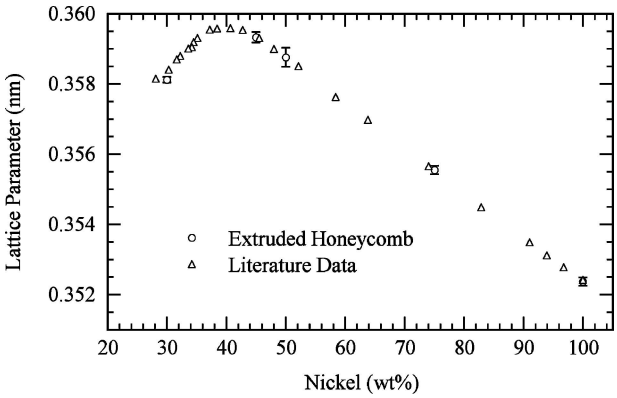

Figure 3 Lattice parameter measurements for Fe-Ni alloys made from reduced oxide precursors compared to literature composition-lattice parameter data [13]. Error bars, based on a 95% confidence interval, represent uncertainty in the lattice parameter calculation.

Lattice parameter calculations for several Fe-Ni alloys made from reduced oxides are shown in Fig. 3 and are compared with literature values [13]. The x-values for extruded and reduced honeycomb in Fig. 3 were assigned based on the as-batched compositions, in which complete reduction and homogenization were assumed. Lattice parameter measurements made from the extruded and reduced strip fall in line with the literature values. The lattice parameter increased from 25 to 40 wt% Ni, after which it decreased linearly to 100% Ni. All samples examined were single-phase γ Fe, Ni with the exception of the Fe 30 wt% Ni sample which showed trace levels of α Fe, Ni in addition to the γ ghase. None of the XRD scans revealed the presence of any metal oxide, even in trace amounts.

The linear thermal expansion of YSZ extruded honeycomb was measured and the CTE (α_T) was calculated. As shown in Fig. 4, the α_T increases linearly between 200 and 1000°C and ranges from roughly 8.5×10^{-6} K^{-1} at room temperature to nearly 12×10^{-6}

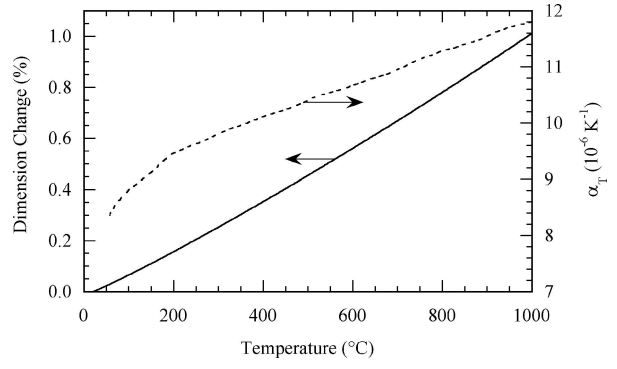

Figure 4 Linear thermal expansion and CTE (α_T) of YSZ extruded honeycomb.

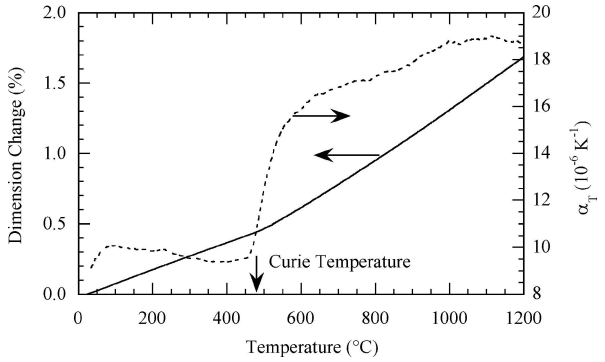

Figure 5 Linear thermal expansion and CTE (α_T) of Fe 50 wt% Ni honeycomb alloy. The indicated Curie temperature of 473°C was measured from the intercept of linear extrapolations of the (nearly) horizontal and vertical portions of the CTE vs. temperature curve.

K^{-1} at 1000°C. Using Equation 3, the CTE (α_m) was calculated to be 10.39×10^{-6} K^{-1} between room temperature and 1000°C. This compares well to other α_m values for YSZ in the literature of 9.8 [9], 10.5 [3], and 10.9×10^{-6} K^{-1} [1].

The measured linear expansion and α_T, for a Fe 50 wt% Ni alloy, are shown in Fig. 5. The CTE decreases slightly from ~75°C up to the Curie temperature of the alloy (473°C) after which there is a prominent increase. The Curie temperature effect is also visible in the measured expansion curve but it is not as pronounced.

The α_T values for each Fe-Ni alloy tested are shown at several temperatures in Fig. 6. The low-temperature invar effect tends to lessen in intensity and shift towards higher nickel contents with increasing temperature. Above 600°C, there is no apparent invar effect across the composition range.

As seen in Fig. 5, the Fe 50 wt% Ni alloy goes through the Curie transformation at ~ 473°C. The Curie temperature represents the end of the magnetic influence on the CTE, and above it the alloy experiences a dramatic increase in CTE over a short temperature interval. Fig. 7 shows a comparison between Curie temperatures from the literature [14] and as measured from extruded honeycomb samples. The measured data show good agreement with literature data, which were measured using dilatometry.

Thermal expansion mismatch values between a given metal alloy and extruded YSZ upon heating from room

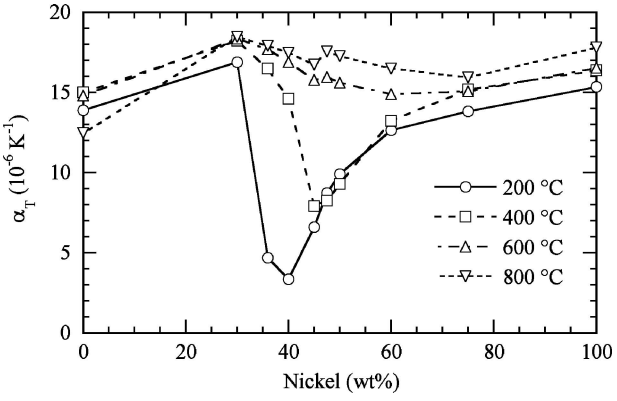

Figure 6 CTE (α_T) of Fe-Ni alloys at several temperatures.

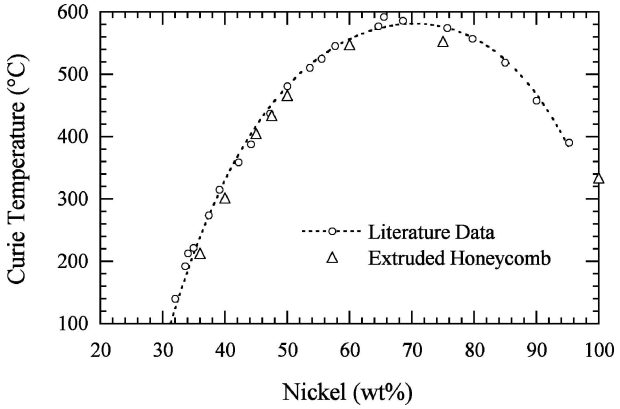

Figure 7 Curie temperature versus composition for Fe-Ni extruded honeycomb samples compared with literature [14] data. Literature data [14], shown with a 4th-order polynomial curve-fit, were measured using dilatometry.

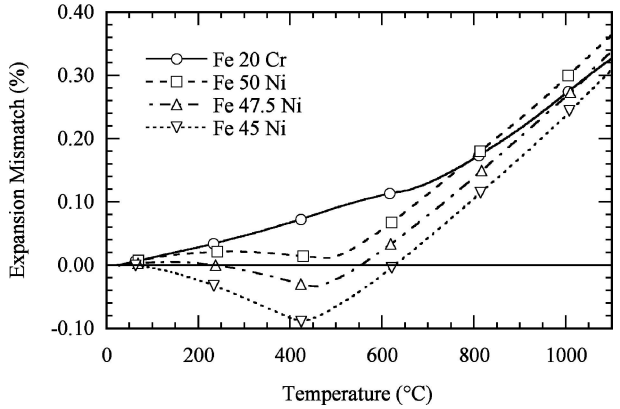

Figure 8 Expansion mismatch between metal alloys and YSZ upon heating from room temperature as calculated using Equation 4. Symbols are used to denote data sets and do not represent individual datum pairs (also true for Figs 9 and 10).

temperature, calculated using Equation 4, are shown in Fig. 8. Both Fe 50 wt% Ni and Fe 47.5 wt% Ni have a lower magnitude mismatch with YSZ compared with Fe 20 wt% Cr up to roughly 1000°C. While the Fe 45 wt% Ni alloy has no net mismatch with YSZ at 650°C, the mismatch between room temperature and 650°C is generally higher in magnitude than the Fe 20 wt% Cr and the Fe 50 and 47.5 wt% Ni alloys.

Thermal expansion mismatch values upon cooling from 1100°C to room temperature, calculated using Equation 5, are shown in Fig. 9. In this case, the materials are assumed to initially be in a stress-free state at 1100°C. Results of thermal mismatch calculations assuming the stress-free state at 600°C are shown in Fig. 10.

4. Discussion

Producing metals directly from oxide precursors may be problematic if complete chemical reduction and homogenization are not achieved. If the sample were homogenized poorly, the XRD pattern would tend to have broad peaks implying a compositional variation. In addition, a larger error would be expected in calculated lattice parameter values. The XRD peaks of all Fe-Ni samples had widths similar to those taken from pure

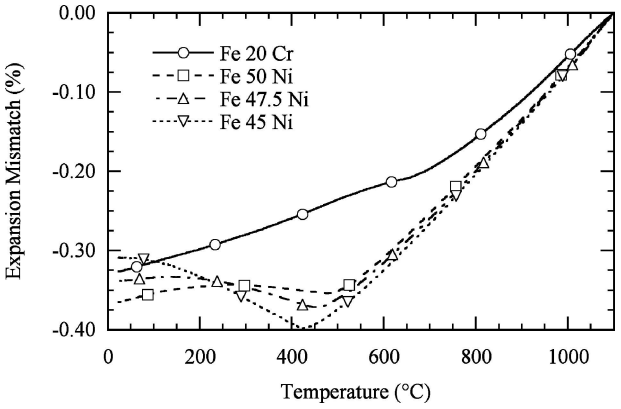

Figure 9 Expansion mismatch due to cooling from 1100°C to room temperature as calculated using Equation 5.

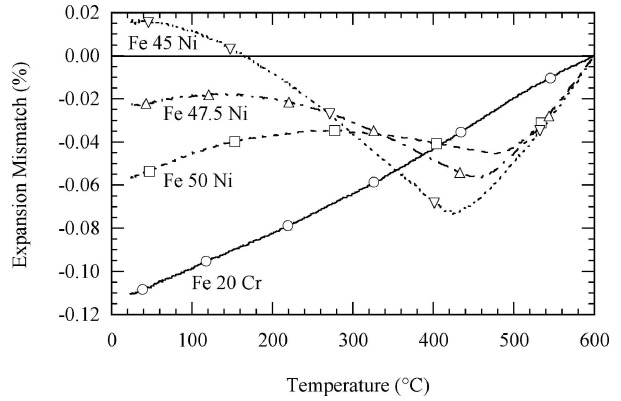

Figure 10 Expansion mismatch due to cooling from 600°C to RT as calculated using Equation 5.

Ni or Fe samples made from the same process. Also, the error in the lattice parameter calculations was typically on the order of 0.1% and did not vary significantly between pure and alloyed samples. Another consideration would be the potential for compositional variation between batches of extruded material. While not systematically studied for all compositions, limited data suggest there was very little variation in properties from batch to batch.

Many studies of potential SOFC interconnects rely on the availability of commercial alloys [1, 10, 15–17] which tends to limit the ability of researchers to explore a wide range of compositions in a given system. A select few studies have used samples produced in-house by means of vacuum induction melting and subsequent hot forging of $\sim$ 10 kg melts [18] or arc-melting of small buttons for oxidation tests [19]. The honeycomb extrusion process used in this work is relatively simple, rapid, cost-effective and allows the researcher to produce a wide range of compositions including Fe-Ni, Fe-Cr [20], and Fe-Ni-Cr, among others. The primary limitation of this fabrication technique is the inability to incorporate low nobility elements such as Al, Mg, or Si.

Of the samples tested using XRD, all were observed to be single-phase austenitic (γ) Fe,Ni with the exception of the Fe 30 wt% Ni sample which showed trace amounts of the ferritic (α) phase. The γ to α transition temperature for a Fe 30 wt% Ni alloy was shown by Jones and Pumphrey [21] to be approximately 50°C, and decreased with increasing nickel content. This makes the presence of the ferritic phase improbable in alloys prepared in this work containing greater than 30 wt% Ni.

The degree of alloy-YSZ thermal mismatch upon heating from room temperature, shown in Fig. 8, is pertinent to SOFC designs that are rigidly joined at room temperature. The Fe 50 wt% Ni and Fe 47.5 wt% Ni alloys have a remarkably low mismatch with YSZ from room temperature up to roughly 500°C, after which the mismatch begins to increase. At the target operation temperature of 700°C, the Fe 45 wt% Ni sample has the lowest mismatch. An open question is whether the more extensive expansion mismatch at 425°C for this composition will cause inter-layer bowing or buckling delamination during heating to the service temperature.

Expansion mismatch values calculated using Equation 5, shown in Figs 9 and 10, are applicable to the process by which the hybrid SOFC stack is produced. In this case, the stack is co-fired at high (>1200°C) temperatures. At some point during cooling from the reduction/sintering heat-treatment, a last stress-free state temperature between the YSZ and the metal is assumed. If the cooling rate from the processing temperature were sufficiently slow to allow for plastic flow, the zero-stress temperature could reasonably assumed to be on the order of 0.4 to 0.5 of the absolute melting temperature (T_M) [22]. This ratio is commonly used to estimate the temperature above which stress relaxation, creep, and other thermally-activated processes can occur. Iron-nickel alloys with between 40 and 50 wt% Ni have melting temperatures in the range of 1725 to 1775 K. Thus a zero-stress temperature is estimated to be 600°C. If, on the other hand, the cooling rate from the processing temperature ($\sim$1200°C) were not sufficiently slow to allow for plastic flow, the zero-stress temperature could be much higher than 600°C. For this case, 1100°C was used as the zero-stress temperature.

Assuming a stress-free temperature of 1100°C, the Fe 20 wt% Cr alloy yields a lower magnitude of expansion mismatch upon cooling to roughly 100 °C. Below 100°C, the Fe 45 wt% Ni alloy has a slightly lower magnitude of mismatch with the YSZ. When considering the entire range of temperatures during cool-down from 1100°C, Fe 20 wt% Cr in general has less mismatch with YSZ. The situation changes when the assumed stress-free temperature is changed to 600°C, as shown in Fig. 10. In this case, the Fe-Ni alloys containing between 45 and 50 wt% Ni have a lower expansion mismatch with YSZ upon cooling to room temperature when compared with Fe 20 wt% Cr.

Of course, the Fe-Ni binary alloys would not possess other desirable properties such as oxidation resistance that the Fe 20 wt% Cr alloy would have. However, these data provide starting points for the development of oxidation-resistant, expansion-matched Fe-Ni-Cr alloys.

5. Conclusions

Metal honeycomb alloys made from reduced oxides can be screened rapidly for potential application as a SOFC interconnect. Chemical composition of the Fe-Ni alloys made via the extrusion and subsequent reduction of metal oxide pastes matched the molar ratios of the mixed oxides based on XRD lattice parameter measurements. Thermal expansion behavior of several Fe-Ni binary alloys was measured and the identified Curie temperatures compare well with literature values. The fabrication method of the SOFC stack must be considered when comparing the expansion behavior potential interconnect alloys. For a hybrid SOFC design, the stress-free temperature must be determined prior to comparing potential interconnect alloys. It was shown that a Fe 50 wt% Ni material has a lower thermal expansion mismatch with YSZ compared with Fe 20 wt% Cr, upon heating from room temperature to 1000°C.

References

1. S. LINDEROTH, P. V. HENDRIKSEN, M. MOGENSEN and N. LANGVAD, *J. Mater. Sci.* **31** (1996) 5077.
2. W. Z. ZHU and S. C. DEEVI, *Mat. Sci. Eng. A-Struct.* **348** (2003) 227.
3. W. J. QUADAKKERS, J. PIRON-ABELLAN, V. SHEMET and L. SINGHEISER, *Mater. High Temp.* **20**(2) (2003) 115.
4. Z. YANG, K. S. WEIL, D. M. PAXTON and J. W. STEVENSON, *J. Electrochem. Soc.* **150**(9) (2003) A1188.
5. N. Q. MINH, *J. Am. Ceram. Soc.* **76**(3) (1993) 563.
6. W. RAUCH, K. J. LEE, J. COCHRAN and M. LIU, in "Solid Oxide Fuel Cells VIII Proceedings of the International Symposium" (The Electrochemical Society, Paris, 2003) p. 1090.
7. S. EISELE, in "Characterization of Material Behavior During the Manufacturing Process of a Co-extruded Solid Oxide Fuel Cell", MS Thesis (Georgia Institute of Technology, 2004).
8. J. COCHRAN, K. HURYSZ, K. J. LEE and T. SANDERS, *Mater. Sci. Forum* **426–432** (2003) 4295.
9. C. S. MONTROSS, H. YOKOKAWA and M. DOKIYA, *Brit. Ceram. T.* **101**(3) (2002) 85.
10. S. LINDEROTH and P. H. LARSEN, in "Materials Research Symposium Proceedings" (Materials Research Society, San Fransisco, 1999) Vol. 575, p. 325.
11. K. M. HURYSZ and J. K. COCHRAN, *J. Eur. Ceram. Soc.* **23** (2003) 2047.
12. J. D. JAMES, J. A. SPITTLE, S. G. R. BROWN and R. W. EVANS, *Meas. Sci. Technol.* **12** (2001) R1.
13. W. B. PEARSON, in "Lattice Spacings and Structures of Metals and Alloys" (Permagon Press, 1958) p. 639.
14. P. CHEVENARD, *Travaux et Memoires du Bureau International des Poids et Mesures* **17** (1927).
15. T. HORITA, Y. XIONG, K. YAMAJI *et al.*, *J. Electrochem. Soc.* **150**(3) (2003) A243.
16. K. HUANG, P. HOU and J. GOODENOUGH, *Solid State Ion.* **129** (2000) 237.
17. W. A. MULLENBERG, S. UHLENBRUCK, E. WESSEL, *et al.*, *J. Mater. Sci.* **38** (2003) 507.
18. T. UEHARA, A. TOJI, K. INOUE *et al.*, in "Solid Oxide Fuel Cells VIII Proceedings of the International Symposium" (The Electrochemical Society, Paris, 2003) p. 915.
19. L. MIKKELSEN and S. LINDEROTH, *Mat. Sci. Eng. A-Struct* **361** (2003) 198.
20. J. H. NADLER, T. H. SANDERS and R. F. SPEYER, *J. Mater. Res.* **18**(8) (2003) 1787.
21. F. W. JONES and W. I. PUMPHREY, *J. Iron Steel I.* **163** (1949) 781.
22. R. W. EVANS and B. WILSHIRE, in "Creep of Metals and Alloys" (The Institute of Metals, 1985) p. 4.

Received 23 September 2004
and accepted 18 January 2005